Mechanics & Industry **24**, 8 (2023)

https://doi.org/10.1051/meca/2023006

Mechanics & Industry

Available online at:
www.mechanics-industry.org

Regular Article

Open Access

Experimental analysis of specific energy with variable deformation volume under sphere oblique impact

Qing-Peng Wang[1,2,*], Shao-Yun Lv[1], Jin-Li Han[1], Heng Wang[1,2], De-Feng Li[1,2], and Zhen-Feng Wang[1,2]

[1] College of Mechanical and Electrical Engineering, Henan Agricultural University, Zhengzhou 450002, China
[2] Henan Provincial Cold Chain Information and Equipment Laboratory for Logistics of Agricultural Products, Henan Agricultural University, Zhengzhou 450002, China

Received: 9 December 2022 / Accepted: 18 February 2023

Abstract. Experiments of a steel sphere oblique impact with a rubber cushion have been proceeded to research the variation laws of the specific energy at interface. The contact surfaces above and under the rubber cushion can be recorded with a thin carbon paper. The parameters of deformation volume and specific energy are analyzed by the developed formulas in different cases of the impact angle, cushion thickness, drop height and sphere diameter. It is found that the deformation volume and related geometrical sizes decrease approximately exponentially with the impact angle, and the volume of the tangential moving part reaches a maximum at 50° or 60°. The variation laws of the specific energy absorption/dissipation in normal are similar to that of the axis length. The tangential specific energy can be divided into three main phases, the first two appear the states of slow increase and plateau, between of them a fluctuating peak exists at 30–40°. In final phase, the energy absorption shows sharp increase, but the energy dissipation first increases and then decreases. In addition, they increase linearly with the drop height and sphere diameter, and an optimum cushion thickness of 4 or 5 mm in the given cases.

Keywords: Specific energy / deformation volume / contact area / oblique impact

1 Introduction

The energy absorption/dissipation at impact interface between a sphere and a flat surface has been attached great importance in various applications, such as mechanical [1–3], agricultural [4,5], mineral [6–8], chemical [9], packaging [10,11] industries, etc. It has notable influences on the system stability, dynamic performance, frictional behavior, etc.

Currently, the commonly used methods to study the energy variation at impact interface can be mainly divided into two classes: continuous and discontinuous descriptions. The first kind is based on the concepts of normal contact force and tangential slip inspired by the theories developed by Hertz and Mindlin [12–15]. There is no energy dissipation for a fully elastic impact. If the loading curve is not coincident with the unloading curve owing to the plastic deformation of the contact materials, and the energy dissipation can be obtained by the area of the hysteresis loop. In addition, the numerical analysis is also a frequently used method to deal with this problem [1,3,9,16]. The second kind is based on a series of phenomenological parameters of the coefficients of restitution (COR) proposed by Newton in 1686, and friction (COF) by Coulomb in 1781, etc. [17,18] This classical method, which can be used to qualitatively characterize the energy variation, is still widely employed because of its simplicity and practicality [17]. Many models have been developed by these parameters to describe the variation of motion states during the impact, representative examples are Brach [19], Foerster [20], Lorenz et al. [21], Mueller et al. [22], Doménech [18], etc.

In previous researches, the geometrical parameters, for instance, maximum dent depth [23–26], contact area [27–29], damage volume [29], etc., have always been used to study the validity of developed model [28], material properties [23–25,27,29], design strategies [26], etc. The compressive strength after impact is frequently used to evaluate the bearing capacity, which can be obviously weakened by the plastic deformation and damage of the contact materials [27,30]. Under low-speed oblique impact, Wang et al. presented a dimensionless index of horizontal dent offset displacement per unit depth [31].

The drawback of the above mentioned parameters is that the concrete value of the energy variation can't be observed visually. To tackle this problem, it has been

* e-mail: welcomewqp@163.com

widely used the parameters directly related with the energy. The test piece, such as cylinder or tube with various section shapes [31–37], was compressed along the axial direction by the top rigid plate with a smooth velocity. Correspondingly, the parameters of total energy absorption (TEA) [1–3,16,31,35,36], specific energy absorption (SEA) [2,3,16,31,33–36], crushing force efficiency (CFE) [2,31,33–36], ratio of horizontal to vertical energy absorption [30], energy-absorbing effectiveness factor [37], etc. were investigated. During these analyses, the crushed volume or mass used to calculate the related energy parameters was assumed to be the whole absorber [36]. However, it is not suitable for low-velocity impact owing to the difficulty obtaining the volume of deformed part [30]. Abd El-baky et al. pointed out the mass can be quantitatively evaluated via the ratio between the deformed and initial lengths [36].

With regard to the sphere oblique impact, it is difficult to obtain the real value of the deformation volume, especially for the spherical impactor, and the crashworthiness indexes can't effectively characterize the variation of impact energy. For these reasons, first of all, based on the geometrical features of the upper and lower contact surfaces, the calculation formulas of the parameters of the deformation volume, specific energy absorption/dissipation in normal and tangential directions are developed. Subsequently, the experiments in different cases of impact angle, cushion thickness, drop height, sphere diameter, etc. are carried out through an apparatus of a steel sphere obliquely impacting a rubber cushion. Finally, the measurements of these parameters are analyzed to obtain the evolution laws.

2 Theory

A sphere is freely dropped from a height h_0 and impacts with a flat surface, as shown in Figure 1a. Based on the law of energy conservation, the effect of the air resistance is neglected, and the relationship between the initial impact velocity and the drop height follows

$$v_0 = \sqrt{2gh_0} \tag{1}$$

where v_0 is initial impact velocity, g is gravitational acceleration, and h_0 is drop height from the release point to the impact point.

In the process of sphere oblique impact, the coefficients of normal restitution and friction change slightly, and they are always regarded as constants [17,18]. According to reference [38], the coefficient of tangential restitution has a relationship with the coefficients of tangential restitution and friction, as

$$e_t = 1 - \mu(1 + e_n)\cot\theta \tag{2}$$

where μ is coefficient of friction, e_n and e_t are respectively coefficients of normal and tangential restitution, θ is impact angle between the flat plate and the horizontal plane.

The energy absorption capacity can be expressed by the maximum strain energy at the end of the loading [28], according to the law of energy conservation, this is equal to the sphere kinetic energy at initial contact point. Based on

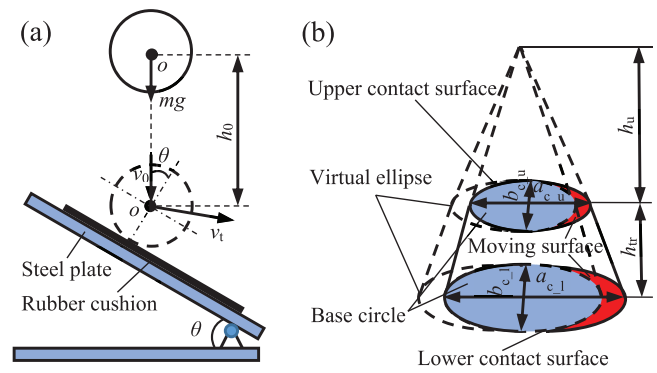

Fig. 1. (a) Oblique impact of sphere with rubber cushion and (b) its deformation volume.

the analysis of kinematics, the normal, tangential and total energy absorption can be given as follow

$$\begin{cases} E_{a\_n} = m(v_0\cos\theta)^2/2 \\ E_{a\_t} = m(v_0\sin\theta)^2/2 \\ E_a = mv_0^2/2 \end{cases} \tag{3}$$

where m is mass of the sphere.

The normal, tangential and total energy dissipation at the impact interface are respectively

$$\begin{cases} \Delta E_{d\_n} = m(v_0\cos\theta)^2\left(1-e_n^2\right)/2 \\ \Delta E_{d\_t} = m(v_0\sin\theta)^2\left(1-e_t^2\right)/2 \\ \Delta E_d = mv_0^2\left[(\cos\theta)^2\left(1-e_n^2\right) + (\sin\theta)^2\left(1-e_t^2\right)\right]/2 \end{cases}. \tag{4}$$

According to Hertz contact theory, there is a linear relationship between the contact area and the deformation, and both the initial values are 0 [28]. Hence, the virtual shape built from successive layers of the contact surface is a cone, as shown in Figure 1b. The relationship of the contact surface with geometrical sizes can be seen in Appendix. The base circle of the contact surface corresponds to a circular cone, on the principle of geometry similarity, the height of the upper circular cone can be expressed as

$$h_u = \frac{b_{c\_u}h_{tr}}{b_{c\_l} - b_{c\_u}} \tag{5}$$

where b_{c_u} and b_{c_l} are respectively the lengths of the minor axis of the upper and lower contact surfaces, h_{tr} is height of the truncated cone.

The lower circular cone consists of the upper and the truncated circular cones. The corresponding volumes are respectively

$$\begin{cases} V_{cc\_u} = \pi h_u b_{c\_u}^2/12 \\ V_{cc\_l} = \pi(h_{tr} + h_u)b_{c\_l}^2/12 \\ V_{cc\_tr} = \pi\left[(h_{tr} + h_u)b_{c\_l}^2 - h_u b_{c\_u}^2\right]/12 \end{cases} \tag{6}$$

where V_{cc_u}, V_{cc_l} and V_{cc_tr} are respectively the volumes of the upper, the lower and the truncated circular cones.

Likewise, the volumes of these elliptic cones are respectively

$$\begin{cases} V_{\mathrm{ec\_u}} = \pi b_{c\_\mathrm{u}} h_u (2a_{c\_\mathrm{u}} - b_{c\_\mathrm{u}})/12 \\ V_{\mathrm{ec\_l}} = \pi b_{c\_\mathrm{l}} (h_{\mathrm{tr}} + h_u)(2a_{c\_\mathrm{l}} - b_{c\_\mathrm{l}})/12 \\ V_{\mathrm{ec\_tr}} = \pi [b_{c\_\mathrm{l}} (h_{\mathrm{tr}} + h_u)(2a_{c\_\mathrm{l}} - b_{c\_\mathrm{l}}) - b_{c\_\mathrm{u}} h_u (2a_{c\_\mathrm{u}} - b_{c\_\mathrm{u}})]/12 \end{cases} \tag{7}$$

where $V_{\mathrm{ec\_u}}$, $V_{\mathrm{ec\_l}}$ and $V_{\mathrm{ec\_tr}}$ are respectively the volumes of the upper, the lower and the truncated elliptic cones, $a_{\mathrm{c\_u}}$ and $a_{\mathrm{c\_l}}$ are respectively the lengths of the major axis of the upper and lower contact surfaces.

Combining equations (6) and (7), the volume caused by the tangential motion is half of the difference between the truncated elliptic and circular cones, i.e.

$$\begin{aligned} V_{m\_\mathrm{tr}} &= (V_{\mathrm{ec\_tr}} - V_{cc\_\mathrm{tr}})/2 \\ &= \frac{\pi}{12}\left[(h_{\mathrm{tr}} + h_u)\left(a_{c\_\mathrm{l}} b_{c\_\mathrm{l}} - b_{c\_\mathrm{l}}^2\right) - h_u\left(a_{c\_\mathrm{u}} b_{c\_\mathrm{u}} - b_{c\_\mathrm{u}}^2\right)\right] \end{aligned} \tag{8}$$

where $V_{\mathrm{m\_tr}}$ is volume of the tangential motion part.

Then, the total deformation volume consists of the truncated circular cone and the tangential moving part, i.e.

$$\begin{aligned} V_{\mathrm{tr}} &= V_{cc\_\mathrm{tr}} + V_{m\_\mathrm{tr}} \\ &= \frac{\pi}{12}\left[a_{c\_\mathrm{l}} b_{c\_\mathrm{l}} (h_{\mathrm{tr}} + h_u) - a_{c\_\mathrm{u}} b_{c\_\mathrm{u}} h_u\right] \end{aligned} \tag{9}$$

The specific energy absorption is an important indicator describing the amount of energy that can be absorbed per unit mass of the contact materials [2,3,16,31,33–36]. Then the normal, tangential and total values can be separately calculated as

$$\begin{cases} \mathrm{SEA}_n = \dfrac{E_{a\_n}}{V_{cc\_\mathrm{tr}}\rho_c} = \dfrac{6m(v_0\cos\theta)^2}{\pi\rho_c\left[(h_{\mathrm{tr}} + h_u)b_{c\_\mathrm{l}}^2 - h_u b_{c\_\mathrm{u}}^2\right]} \\ \mathrm{SEA}_t = \dfrac{E_{a\_t}}{V_{m\_\mathrm{tr}}\rho_c} = \dfrac{6m(v_0\sin\theta)^2}{\pi\rho_c\left[(h_{\mathrm{tr}} + h_u)\left(a_{c\_\mathrm{l}} b_{c\_\mathrm{l}} - b_{c\_\mathrm{l}}^2\right) - h_u\left(a_{c\_\mathrm{u}} b_{c\_\mathrm{u}} - b_{c\_\mathrm{u}}^2\right)\right]} \\ \mathrm{SEA} = \dfrac{E_a}{V_{\mathrm{tr}}\rho_c} = \dfrac{6mv_0^2}{\pi\rho_c[a_{c\_\mathrm{l}} b_{c\_\mathrm{l}}(h_{\mathrm{tr}} + h_{\mathrm{u}}) - a_{c\_\mathrm{u}} b_{c\_\mathrm{u}} h_{\mathrm{u}}]} \end{cases} \tag{10}$$

where ρ_c is density of the softer contact material.

Correspondingly, the specific energy dissipation can be written as

$$\begin{cases} \mathrm{SED}_n = \dfrac{\Delta E_{d\_n}}{V_{cc\_\mathrm{tr}}\rho_c} = \dfrac{6m(v_0\cos\theta)^2\left(1 - e_n^2\right)}{\pi\rho_c[(h_{\mathrm{tr}} + h_u)b_{c\_\mathrm{l}}^2 - h_u b_{c\_\mathrm{u}}^2]} \\ \mathrm{SED}_t = \dfrac{\Delta E_{d\_t}}{V_{m\_\mathrm{tr}}\rho_c} = \dfrac{6m(v_0\sin\theta)^2\left(1 - e_t^2\right)}{\pi\rho_c[(h_{\mathrm{tr}} + h_u)\left(a_{c\_\mathrm{l}} b_{c\_\mathrm{l}} - b_{c\_\mathrm{l}}^2\right) - h_u\left(a_{c\_\mathrm{u}} b_{c\_\mathrm{u}} - b_{c\_\mathrm{u}}^2\right)]} \\ \mathrm{SED} = \dfrac{\Delta E_d}{V_{\mathrm{tr}}\rho_c} = \dfrac{6mv_0^2\left[(\cos\theta)^2\left(1 - e_n^2\right) + (\sin\theta)^2\left(1 - e_t^2\right)\right]}{\pi\rho_c[a_{c\_\mathrm{l}} b_{c\_\mathrm{l}}(h_{\mathrm{tr}} + h_{\mathrm{u}}) - a_{c\_\mathrm{u}} b_{c\_\mathrm{u}} h_{\mathrm{u}}]} \end{cases} \tag{11}$$

3 Test procedure

The schematic set-up of the experimental platform of a steel sphere obliquely impacting with a rubber cushion is shown in Figure 2. It mainly contains the sphere release device, rack section, measuring instruments of drop height, impact angle, etc. The details of the test device have been described by authors to study the interfacial properties during sphere oblique impact [39]. The next work we will do is to introduce the test steps of getting the specific energy with variable deformation volume.

Step 1: A piece of printing paper ($210 \times 150 \times 0.096$ mm) is laid flat onto a rubber cushion (500×255 mm, 1.622 g/cm^3, 70 HA), and then covered a piece of thin carbon paper ($127 \times 90 \times 0.028$ mm). By this means, the upper contact surface between the steel sphere and the rubber cushion can be obtained, and its geometrical sizes including the major and minor axis are measured by a micrometer caliper (0–25 mm, 0.001 mm).

Step 2: Using the same method, when the carbon paper and printing paper are placed underneath the rubber cushion, the sizes of the lower contact surface between the rubber cushion and the steel plate are also obtained.

Step 3: The normal restitution coefficients of the rubber cushion with different thicknesses are obtained by a camera that is transferred into a PC as AVI format video clips. The images of the sphere are recorded at a 720×240 px wide resolution.

Based on the theory presented in Section 2, the volume of deformed part, the energy variation and the specific energy can be calculated by the aforementioned formulas.

4 Experimental results

In this section, the experimental tests have been performed to explore the variation laws of the volume of deformed part and the specific energy. For this purpose, the effects of the impact angle, cushion thickness, drop height, sphere diameter, etc. can be analyzed. In following analysis, the deformation of the steel sphere is neglected because its hardness is much greater than the rubber cushion. For the cushion thickness changed from 1 mm to 5 mm, according to the velocities of sphere before and after the impact, the normal coefficients of restitution are separately 0.12, 0.14, 0.29, 0.34 and 0.33. The tests have been repeated 10 times for each case to ensure the repeatability and reliability of the measurements, and then took an average as the final value.

4.1 Effect of impact angle

When a 30 mm diameter steel sphere was dropped from a height of 400 mm onto a rubber cushion with different thicknesses of 1–5 mm (represented by the notation of t), which was laid flat onto an inclined steel plate. The impact angle can be changed from 0° to 80° at an increment of 10°. For the rubber cushion with thickness of 2 mm, the representative upper and lower contact surfaces at different impact angles are illustrated in Table 1. The

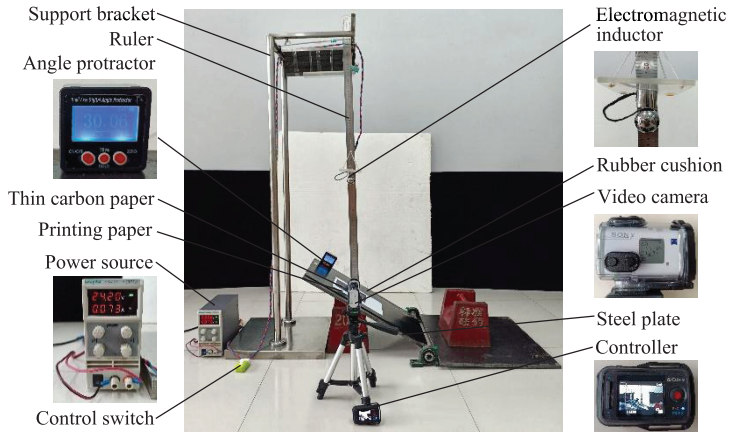

Fig. 2. Test device of sphere oblique impact with rubber cushion.

Table 1. Upper and lower contact surfaces at different impact angles.

Impact angle	0°	10°	20°
Upper surface			
$a_{c\_u}*b_{c\_u}$	9.227*8.949	8.711*8.549	8.516*8.449
Lower surface			
$a_{c\_l}*b_{c\_l}$	10.187*10.150	9.673*9.619	9.616*9.565
Impact angle	30°	40°	50°
Upper surface			
$a_{c\_u}*b_{c\_u}$	8.611*8.395	8.109*7.876	7.994*7.808
Lower surface	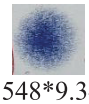		
$a_{c\_l}*b_{c\_l}$	9.548*9.348	9.499*9.283	9.495*9.019
Impact angle	60°	70°	80°
Upper surface			
$a_{c\_u}*b_{c\_u}$	7.958*7.212	7.381*6.294	7.270*5.007
Lower surface			
$a_{c\_l}*b_{c\_l}$	9.442*8.590	9.092*8.167	8.294*6.948

Note: The unit of length of contact surface is mm.

results of geometrical sizes of the contact surface, the volumes of deformed part and the related energy parameters are shown in Figure 3.

For the upper and lower contact surfaces, the sizes of the major and minor axis are respectively shown in Figures 3a and 3b. In comparison, the geometrical lengths of the lower contact surface are obviously greater than that of the upper owing to the stress being transferred and spread downward. For a single contact surface the value of the major axis is apparently larger than that of the minor. When the impact angle θ is smaller than about 30°, the normal component of the impact force plays an important role, and the values of the axis lengths change slightly. However, they increase with the cushion thickness, and reach up to a maximum at 4 or 5 mm thickness. This can be due to the fact that the thicker cushion has more material to bear the applied load, while its effect is limited when the surplus material can't bear the load. For the upper contact

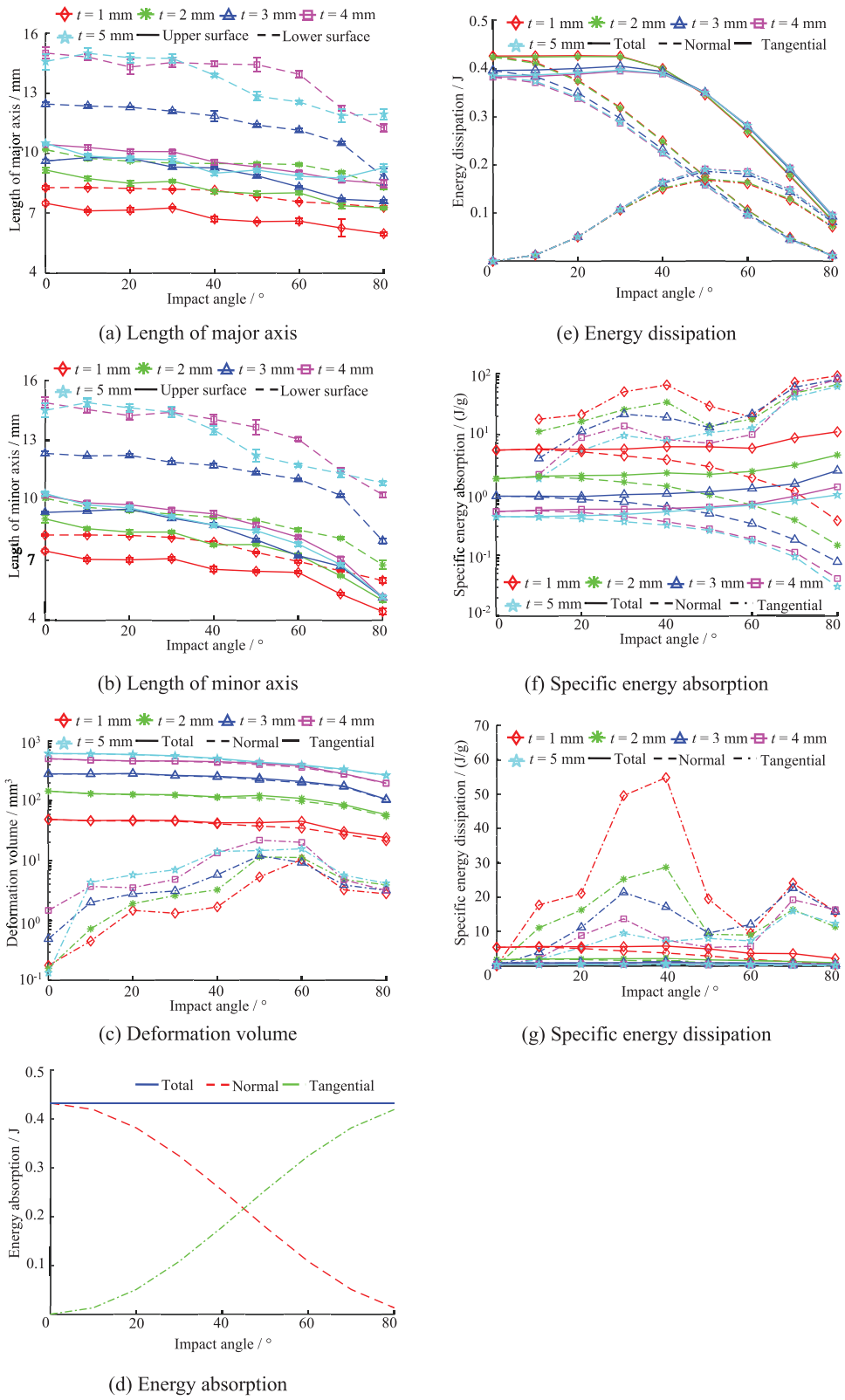

Fig. 3. Geometrical characteristic sizes of contact surfaces, deformation volumes and specific energy parameters at different impact angles.

surfaces the minimum and maximum of the major axis, on average, are separately 7.267 and 10.233 mm, corresponding to the cushion thicknesses of 1 and 4 mm. For the lower contact surfaces, these values are separately 8.259 and 14.785 mm, corresponding to 1 and 5 mm. According to the results presented in [17,18], the sphere can't slide along the plate in this phase, it presents a state of sticking at interface. In this phase, the contact materials can be more easily damaged by the compression.

With the impact angle increasing, the normal component of the impact force decreases gradually, quite the contrary for the tangential. At this point, the axis length starts to clearly decrease, and the impact interface presents a mixed state of micro-slip. After 60° of target inclination, the tangential component of the impact force, which promotes the sphere sliding, turns into a leading role. It is the tangential force that leads to the major axis slowly decreasing. On the whole, the variation laws of the minor axis are similar to that of the major axis except for a significant decline of the value at greater impact angles. At this stage, the tangential component can make a scratch on sphere surface.

The volumes of the total deformation, the truncated circular cone and the tangential moving part are shown in Figure 3c, and the change trends of the first two are consistent with that of the axis length due to a significant action of the normal component. For the volume of tangential moving part, it first increases with a small change rate, and reaches a maximum at the impact angle of 50° or 60°. For example, for the case of the 4 mm thickness cushion the value is 21.984 mm^3 at 50°, which is much smaller than the value of 401.295 mm^3 in normal direction, i.e. about 5% of the total value. Subsequently, it declines because the impact time is so short that the contact materials can't deform just in time.

It can be seen from Figure 3d that the total energy of 0.432 J is conserved at different impact angles, and the normal energy absorption decreases gradually as a cosine curve, while the tangential value increases as a sine curve. Theoretically, there is no tangential energy absorption when the sphere impacts in normal direction. At the other extreme, the normal energy is 0 when the sphere glances off the plate.

Similar to the changes of the energy absorption, the energy dissipation in normal direction shown in Figure 3e decreases when $\theta < 30°$, just the opposite for the tangential. Hence the total value can remain nearly unchanged, the maximum for the 1 mm thickness cushion is 0.427 J. When $30° < \theta < 60°$, the change trends of the normal energy dissipation are similar to that of the energy absorption. Whereas the tangential energy dissipation first increases, and reaches a maximum of 0.16–0.20 J at 50°–60°, which is similar to the change of the corresponding volume. When $\theta > 60°$, the sphere can slide clearly along the impact interface, as seen in Table 1. The energy dissipation in tangential direction is greater than that of the normal, both of them decrease caused by a smaller impact force, thus the total energy dissipation can decrease sharply.

The variations of the specific energy absorption in normal shown in Figure 3f are similar to that of the axis length on account of the synchronous changes between the volume and the energy absorption. For the tangential specific energy, a peak exists at 30–40°, and the value decreases with the cushion thickness increasing. For example, the maximum of the 1 mm thickness cushion at 40° is 65.231 J/g, which is about eight times greater than the minimum of the 5 mm cushion. At this moment, the sphere has a trend of sliding, this is similar to the change of the friction force. With the impact angle increasing, the tangential values keep nearly constant, but an obvious increase starts from 60° because of a small tangential moving volume. For the total specific energy, it is almost invariable at smaller impact angles, for the same case the value is 6.228 J/g, i.e. about 10% of the tangential value. Then it increases because the tangential specific energy has a greater influence than the normal. For different cushion thicknesses the corresponding change law is contrary to that of the axis length, and an optimum value exists at 4 or 5 mm. For example, the change rates of the specific energy absorption at 40° for the different cushion thicknesses, ranging from 1 mm to 5 mm, are separately 63.10%, 54.57%, 43.10% and 11.95%, i.e. the ability absorbed the applied energy decreases with the cushion thickness. The same results can be found in [3]. The change laws of the specific energy dissipation shown in Figure 3g are similar to that of the specific energy absorption. The main differences are that the total specific energy dissipation starts to decrease at more oblique angles (> 60° here) due to a short contact duration, and the tangential values decrease after 70°.

4.2 Effect of drop height

A 30 mm diameter steel sphere fell from different drop heights onto a rubber cushion with different thicknesses of 1–5 mm, which was laid flat onto a steel plate inclined at 30°. The results of the geometry and energy parameters are presented in Figure 4.

Figure 4a shows the sizes of the major axis for the upper and lower contact surfaces at different drop heights changed from 100 mm to 600 mm, i.e. the impact velocity changing from 1.40 m/s to 3.43 m/s. For the 1 mm thickness cushion, they increase nearly linearly with the proportional coefficients of 0.0039 and 0.0035, and their increments are separately 2.209 and 1.782 mm, i.e. 35.72% and 26.69%. This is because the impact energy increases with the drop height, and the cushion material at the bottom constrained by the steel plate can't produce a shearing motion compared to that at the top. The influences of the cushion thickness are similar to that mentioned in Section 4.1. Aside from the smaller values, the same change trends for the minor axis are shown in Figure 4b. The changes of the volume shown in Figure 4c are approximately consistent with that of the axis length. The big difference is that the volumes of the deformed part for the 5 mm thickness cushion are greater than the 4 mm

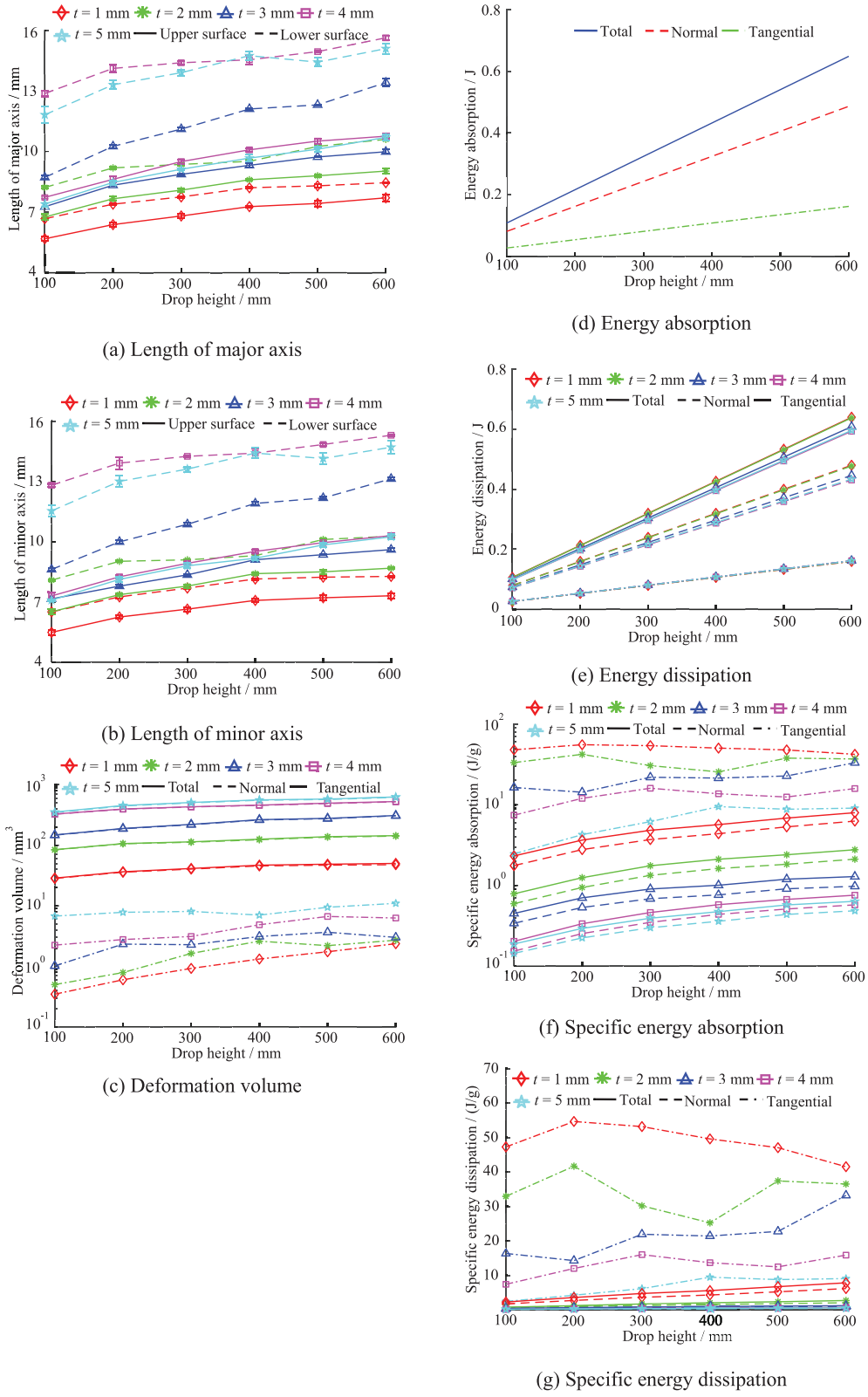

Fig. 4. Geometrical characteristic sizes of contact surface, deformation volume and specific energy parameters at different drop heights.

thickness. The cause can be that the increment of the volume by increasing the cushion thickness is greater than the decrement generated by the axis length.

The energy absorption shown in Figure 4d increases with a similar change trend, and the increase rate in normal direction is obviously greater than that of the tangential. In other words, during the oblique impact, the sphere first comes into a state of compression, then a motion of slip or roll will be happened when the tangential driving force can overcome the interfacial friction. Likewise, the energy dissipation is shown in Figure 4e. These change laws can also be deduced from equations (1)–(4).

Figure 4f depicts the curves of the specific energy absorption, the results of the normal are close to the total. Both of them show a linear increase with the drop height. When the drop height changes from 100 mm to 600 mm, the corresponding increase rates for the 1 and 5 mm thickness cushions are separately 255.82% and 237.26%. By contrast, the values of the tangential component are at least an order of magnitude greater than the normal component, because the tangential impact energy may be applied to a small deformation volume. For the thinner cushions, such as 1 and 2 mm, the effects of the drop height on the tangential parameters are very little owing to the nearly synchronous variation of the deformation volume and the energy absorption. However, a linear increase for the thicker cushion because the increasing impact energy corresponds to a nearly constant volume. The specific energy dissipation shown in Figure 4g has a similar change trend except for slightly small results.

4.3 Effect of sphere diameter

A sphere with different diameters was dropped from a height of 400 mm onto a rubber cushion. The results are laid out in Figure 5.

The geometrical parameters of the axis lengths and the volumes, as shown in Figures 5a–5c, all increase nearly linearly when the sphere diameter increases from 20 mm to 45 mm, correspondingly, the increasing gravitational potential energy makes the impact force grow greater. Comparatively, the changes of the volumes are similar to that mentioned above. Figures 5d–5e depict the curves of the energy absorption and dissipation, which all increase exponentially due to a third power relationship between the energy/mass and the sphere diameter. There is a discernible difference in various cushion thicknesses for the normal and total energy dissipation, while the tangential is virtually unnoticeable. The specific energy absorption/dissipation shown in Figures 5f–5g also increase nearly linearly with the sphere diameter. The increase rates of the normal and the total almost hardly change, but the values in tangential decrease. This is because the contact materials can absorb the applied energy until they reach a state of saturation no matter in normal or tangential direction. If there's some surplus energy, i.e. the larger the sphere diameter, the more energy needs to be transferred, the contact materials can be more likely to produce yield, plastic deformation, failure, etc. in normal direction, and slip, scratch, etc. in tangential direction. Obviously, the thinner cushion has no enough material to absorb the applied energy, that is to say, the unit mass material needs to absorb more energy, so it can be more easily destroyed.

5 Discussion

The specific energy absorption or dissipation during the impact between the sphere and the rubber cushion is not always constant, and related with the impact angle, cushion thickness, drop height, sphere diameter, etc. The influence laws on the energy parameters can be included in Table 2.

Based on the variations of the geometrical characteristic sizes and the specific energy, it can be divided into three main phases by two critical impact angles of θ_{c1} and θ_{c2}, as shown in Figure 6.

(I) When $\theta < \theta_{c1}$, the normal component of the impact force plays an important role, the specific energy slightly decreases just because of smaller variations of the applied energy and the deformation volume. In this phase, the sphere can't move along the plate owing to a larger friction force [17], i.e. the tangential component of the impact energy corresponds to a small volume, which can lead to a greater tangential specific energy. All these parameters decrease with the cushion thickness increasing. Such behavior is due to the fact that the thicker cushion tends to be deformed more easily, a larger deformation volume is obtained, and the impact energy can be absorbed effectively. Otherwise, the contact materials will be deformed plastically, damaged or fractured, etc. A fluctuating peak of the specific energy exists at the first critical angle of $\theta_{c1,}$ where the maximum static friction force at interface is larger than the sliding friction force. We can deduce the critical angle will become large with the friction coefficient. Further, the thinner the cushion, the higher the peak. The reason is that no adequate contact material and time can be used to absorb and dissipate the applied energy [29]. Actually, it is similar to an underdamped vibration system. The small damping gets a larger vibration amplitude, on the contrary, the large damping prompts the vibrating system to be steady.

(II) When $\theta_{c1} < \theta < \theta_{c2}$, the normal component of the impact force decreases with the impact angle. The geometrical sizes of the upper and lower contact surfaces become small little by little, and the corresponding volume of the truncated circular cone decreases. For a thicker cushion, the deformation volume can increase more rapidly, and the normal energy parameters decrease gradually. Although the tangential component of the impact force increases gradually, the sphere presents a state of micro-slip owing to a large interfacial friction [17,18]. In this phase, the sizes of the major and minor axis change synchronously. Correspondingly, the variations of the tangential energy and volume are approximately identical. Hence, the parameters of the specific energy absorption and dissipation are nearly constant.

The variation laws of the specific energy absorption and dissipation are consistent with the coefficient of restitution. It can be seen that the ability to dissipate the applied energy declines with the cushion thickness increasing, and

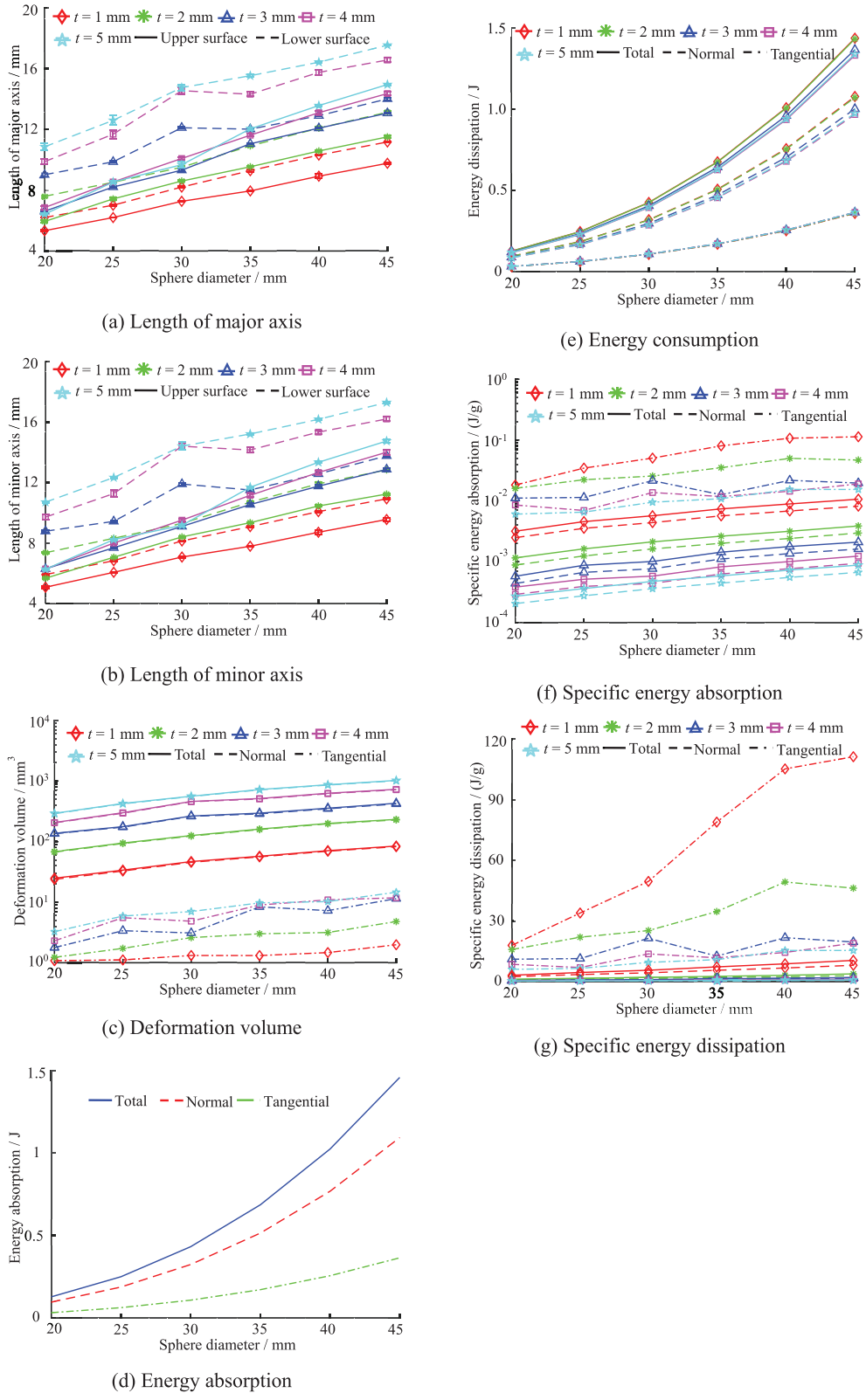

(a) Length of major axis

(b) Length of minor axis

(c) Deformation volume

(d) Energy absorption

(e) Energy consumption

(f) Specific energy absorption

(g) Specific energy dissipation

Fig. 5. Geometrical characteristic sizes of contact surface, deformation volume and specific energy parameters at different sphere diameters.

Table 2. Relationships of normal and tangential specific energy parameters with different influence factors.

Influence factor	SEA_n	SEA_t	SED_n	SED_t
Impact angle ↑	↓	↑	↓	↑→↓
Cushion thickness ↑	↓→—	↓→—	↓→—	↓→—
Drop height ↑	↑	—	↑	—
Sphere diameter ↑	↑	↑	↑	↑

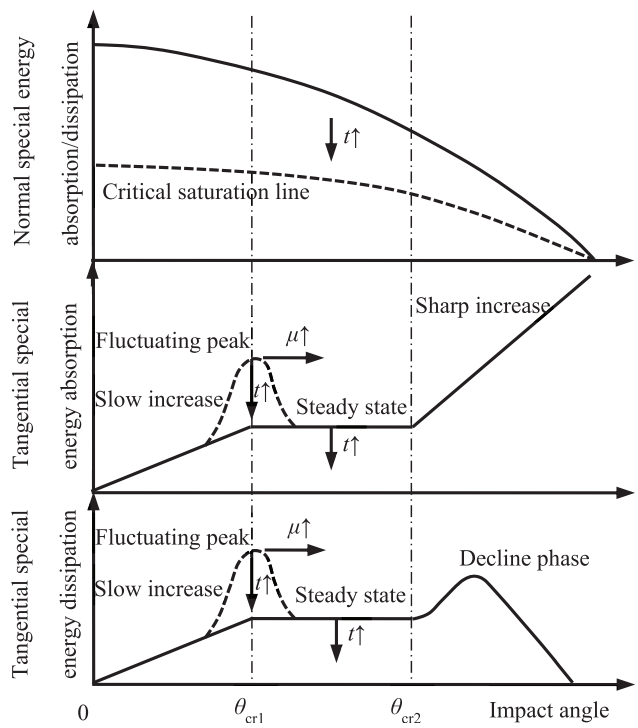

Fig. 6. Change laws of special energy parameters.

there is an optimum cushion thickness of 4 or 5 mm for the given loads. This is because the thinner cushion can't effectively bear or absorb the impact energy, and more energy will be dissipated in the form of plastic deformation of the contact materials, frictional heat, chemical reaction, etc. Conversely, when the cushion thickness increases, more materials can be deformed to absorb the applied energy, meanwhile, the corresponding energy dissipation decreases. From this, a thicker cushion is not necessarily beneficial to the enhancement of energy absorption/dissipation capacity, when the material can bear the applied energy without yielding or damage.

(III) When $\theta > \theta_{c2}$, the normal component of the impact force decreases rapidly, and the same change trend for the geometrical sizes and deformation volumes. Hence, the normal specific energy decreases. In theory, there is no normal energy and deformation volume at 90°, i.e. the normal specific energy is 0. In tangential direction, the specific energy increases sharply due to the increasing absorbed energy and the decreasing volume. On the contrary, the tangential dissipated energy decreases, which leads to the specific energy dissipation first increasing and then decreasing.

6 Conclusions

The parameters of the specific energy with variable volume of deformed part are proposed in this paper. An apparatus of a sphere oblique impact with a rubber cushion has been used to obtain the geometrical sizes of the upper and lower contact surfaces, and the variation laws of the deformation volume and the specific energy can be analyzed in different cases. It is concluded that the deformation volumes and related geometrical sizes decrease approximately exponentially with the impact angle, and the volume of the tangential moving part reaches a maximum at the impact angle of 50° or 60°, which is only 5% of the total value. The variation laws of the specific energy absorption/dissipation in normal are similar to that of the axis length. The specific energy in tangential can be divided into three main phases. The first two appear the states of slow increase and plateau, between of them a fluctuating peak exists at the impact angle of 30–40°, where the value is about 10 times the total. For $\theta > \sim 60°$, the energy absorption shows sharp increase, but the energy dissipation first increases and then decreases. In addition, these parameters increase nearly linearly with the drop height and sphere diameter, and an optimum cushion thickness of 4 or 5 mm in the given cases.

Nomenclature

a	major axis of contact surface
b	minor axis of contact surface
e	coefficient of restitution
g	gravitational acceleration
h	height
m	mass
v	impact velocity
A	area
E	energy
SEA	specific energy absorption
SED	specific energy dissipation
V	volume
θ	impact angle
μ	friction coefficient
ρ	density

Subscripts

a	absorption
bc	base circle
c	contact
cc	circular cone
cr	critical
e	ellipse
ec	elliptic cone
d	dissipation
l	lower
m	motion
n	normal
t	tangential
tr	truncated cone
u	upper
0	initial state

Conflict of interest

The authors declare no potential conflicts of interest with respect to the research, authorship and publication of this article.

Financial support

This research is jointly funded by the China Postdoctoral Science Foundation (No. 204225); Educational Committee of Henan Province of China (No. 20B210010); Commission of Science Technology of Henan Province of China (No. 202102110127); and Henan Agricultural University (Nos. 30500461, 202210466058).' to 'Commission of Science Technology of Henan Province of China (Nos. 202102110127, 202210466058); and Henan Agricultural University(No. 30500461). The project of No. 202210466058 was submitted to Henan Agricultural University. Later, it was submitted to Commission of Science Technology of Henan Province of China by school science and technology office, and have been approved at present.

Appendix. The relationship of contact surface with geometrical sizes

The contact surface is composed of the base circle and the moving surface, and the virtual ellipse is formed by symmetrically setting the two moving surfaces against adjoining sides of the base circle. The three shapes have the same size, i.e.

$$\begin{cases} b_{c\_u} = d_{bc\_u} = b_{e\_u} \\ b_{c\_l} = d_{bc\_l} = b_{e\_l} \end{cases}, \tag{A.1}$$

where $d_{\mathrm{bc\_u}}$ and $d_{\mathrm{bc\_l}}$ are respectively the diameters of the upper and lower base circles, $b_{\mathrm{e\_u}}$ and $b_{\mathrm{e\_l}}$ are respectively the minor axis of the upper and lower virtual ellipses.

The major axis of the virtual ellipse can be calculated by

$$\begin{cases} a_{e\_u} = 2a_{c\_u} - b_{c\_u} \\ a_{e\_l} = 2a_{c\_l} - b_{c\_l} \end{cases}. \tag{A.2}$$

The areas of the base circle are respectively

$$\begin{cases} A_{bc\_u} = \pi b_{c\_u}^2/4 \\ A_{bc\_l} = \pi b_{c\_l}^2/4 \end{cases}, \tag{A.3}$$

where $A_{\mathrm{bc\_u}}$ and $A_{\mathrm{bc\_l}}$ are respectively the areas of the upper and lower base circles.

As before, the areas of the virtual ellipse at the upper and lower contact surfaces are respectively

$$\begin{cases} A_{e\_u} = \pi b_{c\_u}(2a_{c\_u} - b_{c\_u})/4 \\ A_{e\_l} = \pi b_{c\_l}(2a_{c\_l} - b_{c\_l})/4 \end{cases}, \tag{A.4}$$

where $A_{\mathrm{e\_u}}$ and $A_{\mathrm{e\_l}}$ are respectively the areas of the upper and lower virtual ellipses.

References

[1] Y.C. Duan, X. Xie, T. Zou, T.T. Wang, Mechanical response of CFRP laminates subjected to low-velocity oblique impact, Appl. Compos. Mater. **29**, 1105–1124 (2022)

[2] A.B. Nia, A.F. Nejad, X. Li, A. Ayob, M.Y. Yahya, Energy absorption assessment of conical composite structures subjected to quasi-static loading through optimization based method, Mech. Ind. **21**, 113 (2020)

[3] Z.G. Wang, X.X. Wang, K. Liu, J. Zhang, Z. Lu, Crashworthiness index of honeycomb sandwich structures under low-speed oblique impact, Int. J. Mech. Sci. **208**, 106683 (2021)

[4] H. Fu, M. Karkee, L. He, J.L. Duan, Q. Zhang, Bruise patterns of fresh market apples caused by fruit-to-fruit impact, Agronomy-Basel **10**, 59 (2020)

[5] P. Komarnicki, R. Stopa, Ł. Kuta, D. Szyjewicz, Determination of apple bruise resistance based on the surface pressure and contact area measurements under impact loads, Comput. Electron Agric. **142**, 155–164 (2017)

[6] Y. Ye, Y.W. Zeng, S.F. Cheng, H. Sun, X. Chen, Numerical investigation of rock sphere breakage upon oblique impact: effect of the contact friction coefficient and impact angle, Comput. Geotech. **136**, 104207 (2021)

[7] X.Y. Ye, D.M. Wang, X.Y. Zhang, C.F. Zhang, W. Du, X.Y. Su, G. Li, Projectile oblique impact on granular media: penetration depth and dynamic process, Granul. Matter. **23**, 48 (2021)

[8] J. Xie, M. Dong, S. Li, Y. Mei, Y. Shang, An experimental study of fly ash particle oblique impact with stainless surfaces, J. Aerosol. Sci. **123**, 27–38 (2018)

[9] A.D. Renzo, F.P.D. Maio, Comparison of contact-force models for the simulation of collisions in DEM-based granular flow codes, Chem. Eng. Sci. **59**, 525–541 (2004)

[10] M. Xia, X.X. Zhao, X.P. Wei, W.L. Guan, L.C. Mao, Impact of packaging materials on bruise damage in kiwifruit during free drop test, Acta Physiolog. Plant. **42**, 119 (2020)

[11] Y. Sasaki, T. Orikasa, N. Nakamura, K. Hayashi, T. Shiina, Lifecycle assessment of peach transportation considering trade-off between food loss and environmental impact, Int. J. Life Cycle Asses. **26**, 822–837 (2021)
[12] N. Maw, J.R. Barber, J.N. Fawcett, The rebound of elastic bodies in oblique impact, Mech. Res. Commun. **4**, 17–22 (1977)
[13] C. Thornton, Z. Ning, A theoretical model for the stick/bounce behaviour of adhesive, elastic-plastic spheres, Powder Technol. **99**, 154–162 (1998)
[14] W.J. Stronge, R. James, B. Ravani, Oblique impact with friction and tangential compliance, Philos. Trans. R Soc. A **359**, 2447–2465 (2001)
[15] P. Müller, T. Pöschel, Oblique impact of frictionless spheres: on the limitations of hard sphere models for granular dynamics, Granul. Matter **14**, 115–120 (2012)
[16] M.S. Rad, H. Hatami, R. Alipouri, A.F. Nejad, F. Omidinasab, Determination of energy absorption in different cellular auxetic structures, Mech. Ind. **20**, 302 (2019)
[17] H. Dong, M.H. Moys, Experimental study of oblique impacts with initial spin, Powder Technol. **161**, 22–31 (2006)
[18] A. Doménech-Carbó, Independent friction-restitution approach to analyze anomalies in normal kinematic restitution in oblique impact, Mech. Res. Commun. **113**, 103699 (2021)
[19] R.M. Brach, Friction, restitution, and energy loss in planar collisions, J. Appl. Mech. Trans. ASME **51**, 164–170 (1984)
[20] S.F. Foerster, M.Y. Louge, H. Chang, K. Allia, Measurements of the collision properties of small spheres, Phys. Fluids **6**, 1108–1115 (1994)
[21] A. Lorenz, C. Tuozzolo, M.Y. Louge, Measurement of impact properties of small, nearly spherical particles, Exp. Mech. **37**, 292–298 (1997)
[22] P. Mueller, S. Antonyuk, M. Stasiak, J. Tomas, S. Heinrich, The normal and oblique impact of three types of wet granules, Granul. Matter **13**, 455–463 (2011)
[23] K. Yuan, K. Liu, Z.G. Wang, M.Z. Yang, An investigation on the perforation resistance of laminated CFRP beam and square plate, Int. J. Impact Eng. **157**, 103967 (2021)
[24] D. Wowk, T. Reyno, R. Yeung, C. Marsden, An experimental and numerical investigation of core damage size in honeycomb sandwich panels subject to low-velocity impact, Compos. Struct. **254**, 112739 (2020)
[25] K. Arakawa, Effect of dynamic friction on oblique impact deformation of elastic spheres, Tribol. Int. **139**, 55–58 (2019)
[26] R. Olsson, Engineering method for prediction of impact response and damage in sandwich panels, J. Sandw Struct. Mater **4**, 3–29 (2002)
[27] D. Feng, F. Aymerich, Damage prediction in composite sandwich panels subjected to low-velocity impact, Compos. Part A Appl. S **52**, 12–22 (2013)
[28] M.R. Brake, An analytical elastic plastic contact model with strain hardening and frictional effects for normal and oblique impacts, Int. J. Solids Struct. **62**, 104–123 (2015)
[29] M. Messaadi, G. Kermouche, P. Kapsa, Numerical and experimental analysis of dynamic oblique impact: effect of impact angle, Wear **332–333**, 1028–1034 (2015)
[30] R. Bai, J. Guo, Z. Lei, D. Liu, Y. Ma, C. Yan, Compression after impact behavior of composite foam-core sandwich panels, Compos. Struct. **225**, 111181 (2019)
[31] Z.G. Wang, J. Zhang, Z.D. Li, C. Shi, On the crashworthiness of bio-inspired hexagonal prismatic tubes under axial compression, Int. J. Mech. Sci. **186**, 105893 (2020)
[32] M. Hosseini, H. Hatami, Elastic-plastic analysis of bending moment − axial force interaction in metallic beam of T-section, J. Appl. Comput. Mech. **5**, 162–173 (2019)
[33] T.N. Tran, A. Baroutaji, Q. Estrada, A. Arjunan, H. Le, N.P. Thien, Crashworthiness analysis and optimization of standard and windowed multi-cell hexagonal tubes, Struct. Multidiscip. O **63**, 2191–2209 (2021)
[34] M. Kotełko, M. Ferdynus, J. Jankowski, Energy absorbing effectiveness – different approaches, Acta Mech. Autom. **12**, 54–59 (2018)
[35] J.W. Xiang, J.X. Du, Energy absorption characteristics of bio-inspired honeycomb structure under axial impact loading, Mat. Sci. Eng. A **696**, 283–289 (2017)
[36] M.A. Abd El-baky, D.A. Hegazy, M.A. Hassan, Advanced thin-walled composite structures for energy absorption applications, Appl. Compos. Mater. **29**, 1195–1233 (2022)
[37] N. Jones, Energy-absorbing effectiveness factor, Int. J. Impact Eng. **37**, 754–765 (2010)
[38] R. Sondergaard, K. Chaney, C.E. Brennen, Measurements of solid spheres bouncing off flat plate, J. Appl. Mech. Trans. ASME **57**, 694–699 (1990)
[39] Q.P. Wang, Z.F. Wang, H. Wang, D.F. Li, X.K. Gao, G.Y. Xu, Experimental analysis of interfacial properties of sphere oblique impact with initial spin, J. Theor. Appl. Mech-Pol. **60**, 213–225 (2022)

Cite this article as: Q.-P. Wang, S.-Y. Lv, J. Han, H. Wang, D.-F. Li, Z.-F. Wang, Experimental analysis of specific energy with variable deformation volume under sphere oblique impact, Mechanics & Industry **24**, 8 (2023)